ADAPTIVE VIBRATION CONTROL IN ROTATING MACHINE USING BEARING WITH SHAPE MEMORY ALLOY SPRINGS

Silva, José Adriano Brito da, jbadriano@gmail.com
Mesquita, Alexandre Luiz Amarante, alexmesq@ufpa.br
Federal University of Pará, Faculty of Mechanical Engineering, Belém-PA, Brazil, 66075-110

Da Silva, Edson Paulo, dasilva@unb.br
University of Brasília, Department of Mechanical Engineering, Brasília-DF, Brazil, 70910-900

Abstract. Shape Memory Alloys (SMA) are classified as smart materials mainly due to their ability to recover their original shape upon heating. In addition, they present large recovery forces and damping capacity when compared to traditional materials. Despite a great number of papers dealing with SMA abilities applied to vibration control in structures, there are only a few reports about applications of SMA in rotordynamics. This paper focuses basic aspects of the application of SMA for vibration control in rotating machines. It is divided into two parts. The first one describes the implementation of an algorithm to predict the behavior of SMA springs during the activation (heating) and de-activation (cooling) processes. The results show the elastic range in low-temperature (martensite) and high-temperature (austenite) phase and the variation of the stiffness between these two states. A well-know one-dimensional thermomechanical constitutive model for SMA was considered for the simulations. In the second part we present two case studies which deal with vibration control in rotors subjected to unbalance forces by menas of a finite element model to compute the complex response of the system. It has been used the SMA spring's linear elastic characteristics determined in the first part of this work and some comparisons are made in terms of vibration amplitude reduction and application of the activation process of the SMA spring to suppress unwanted vibrations in the rotating system.

Keywords: shape memory alloys, vibration control, adaptive control, rotordynamics.

1. INTRODUCTION

Shape Memory Alloys (SMA) are metallic alloys that can undergo martensitic phase transformations as a result of applied thermomechanical loads and are capable of recovering a original shape when heated above a certain temperature. In addition, they present large recovery forces and damping capacity when compared to traditional materials. These smart materials have unique properties which are not present in many materials traditionally used in engineering applications. Accordingly, their use introduces new design capabilities, which make it possible to improve device performance as well as to propose innovative solutions (Auricchio *et al.*, 1997).

Extensive recent research has shown that shape memory alloy components can be successfully integrated within structural elements in order to improve, enhance, or control both their static and dynamic characteristics (Zak *et al.*, 2003). However, despite large number of papers that deal with vibration control using SMA in structures, there are only a few reports on vibration control for a rotating machine using SMA (Iwata and Nonami, 1983; Zak *et al.*, 2000; He *et al.*, 2007a; He *et al.*, 2007b).

The present work deals with numerical simulations of vibration control in rotating systems by means of SMA. The paper is divided into two parts. The first one consists of implementation of an one-dimensional algorithm to predict the behavior of SMA springs during the activation and de-activation processes. It has been possible by means of the results generated to visualize the elastic limits in low-temperature (martensite) and high-temperature (austenite) phases and the variation of the stiffness between the two states. Furthermore, in the second part, some numerical simulations of a rotor system with two disks supported at both ends by flexible bearings have been made. A set of SMA springs was placed at the right-hand end the shaft, externally to bearing, and then the vibration control is accomplished by altering the bearing stiffness through SMA springs activation (austenite phase) or de-activation (martensite phase). Subsequently, the numerical model is assumed to be asymmetrical in relation to disks position and bearing stiffness. The results show that SMA springs may be used to suppress the backward and mixed operational modes that arise from this new arrangement.

2. MACRO-MECHANICAL CONSTITUTIVE MODELS

To represent the SMA thermomechanical behavior two well known models were considered: the Liang and Rogers' model (1990) and the Brinson's model (1993).

2.1. Liang and Rogers' Model

The Liang and Rogers' model (Liang and Rogers, 1990) is based on the model proposed by Tanaka (1986). However, to characterize the evolution of the martensite fraction a cosine function is employed instead of an

exponential one. In their work they presented a methodology for determination of the evolution equation and discussed it experimentally. Hence, the constitutive equation which describes the stress-strain-temperature-martensite fraction for the Liang and Rogers' model is defined as follows (Liang and Rogers, 1990):

$$\sigma - \sigma_0 = D(\varepsilon - \varepsilon_0) + \Omega(\xi - \xi_0) + \Theta(T - T_0) \tag{1}$$

where σ, D, ε, Ω, ξ, Θ and T represent the stress, Young's modulus, phase-transformation tensor, martensite fraction, thermo-elastic tensor and temperature respectively. The subscript "0" represents the initial conditions before transformation. The relation between D and Ω is described as $\Omega = -\varepsilon_L D$, where ε_L is the maximum recoverable deformation for a SMA material. Thus, the evolution equations are expressed for direct (austenite → martensite) and reverse (martensite → austenite) transformation according to situations described below.

- Variable Stress and Constant Temperature: $A \to M$ Transformation

$$\xi = \frac{1-\xi_A}{2}\cos(a_M(T-M_f)+b_M\sigma) + \frac{1+\xi_A}{2} \tag{2}$$

- Variable Stress and Constant Temperature: $M \to A$ Transformation

$$\xi = \frac{\xi_M}{2}\cos(a_A(T-A_S)+b_A\sigma) + 1 \tag{3}$$

where M_f and A_S are the temperatures corresponding to martensite finish and austenite start, respectively. The constant parameters a_A, a_M, b_A, b_M and Θ are defined by Liang (1990) and the subscripts M and A indicate the martensite and austenite states, respectively.

One of the main limitations of this model is that it describes only the martensite transformation into austenite and vice-versa, and it is not able to describe the re-orientation of twinned martensite in temperatures below M_S (martensite finish). Brinson (1993) proposed to separate the martensite volume fraction into temperature-induced and stress-induced components, as explained in the following section.

2.2. Brinson's Model

The Brinson's model (Brinson, 1993), as well as the Liang and Rogers's model (Liang and Rogers, 1990), is based on the model proposed by Tanaka (1986). One of the main differences between them is that Brinson's model comprises all the temperature range, from M_f up to A_f (austenite finish). In addition, this model distinguishes the martensite fractions in its components induced by stress and temperature, i.e.:

$$\xi = \xi_S + \xi_M \tag{4}$$

where ξ_S is the single-variant fraction and ξ_M the multi-variant fraction. The constitutive equation considering the new definition on martensite fractions is written as:

$$d\sigma = D d\varepsilon + \Omega_S d\xi_S + \Omega_M d\xi_M + \Theta dT \tag{5}$$

and the evolution laws for the Brinson's model are defined for different temperature range as:

- $T > M_S$ – Direct Transformation for Single-variant Martensite

$$\xi_S = \frac{1-\xi_{S0}}{2}\cos\left\{\frac{\pi}{\sigma_s^{cr}-\sigma_f^{cr}}\left[\sigma-\sigma_f^{cr}-C_M(T-M_S)\right]\right\} + \frac{1+\xi_{S0}}{2} \tag{6}$$

$$\xi_M = \xi_{M0} - \frac{\xi_{M0}}{1-\xi_{S0}}(\xi_S - \xi_{S0}) \tag{7}$$

- $T < M_S$ – Direct Transformation for Single-variant Martensite

$$\xi_S = \frac{1-\xi_{S0}}{2}\cos\left\{\frac{\pi}{\sigma_s^{cr}-\sigma_f^{cr}}\left[\sigma-\sigma_f^{cr}\right]\right\}+\frac{1+\xi_{S0}}{2} \tag{8}$$

$$\xi_M = \xi_{M0}-\frac{\xi_{M0}}{1-\xi_{S0}}\left(\xi_S-\xi_{S0}\right) \tag{9}$$

if $M_f < T < M_S$ and $T < T_0$, then:

$$\Delta_{T\xi} = \frac{1-\xi_{M0}}{2}\left\{\cos\left[a_M\left(T-M_f\right)\right]+1\right\} \tag{10}$$

otherwise, $\Delta_{T\xi} = 0$.

- $T > A_S$ – Reverse Transformation of Single-variant Martensite into Austenite

$$\xi = \frac{\xi_{S0}}{2}\left\{\cos\left[a_A\left(T-A_S-\frac{\sigma}{C_A}\right)\right]+1\right\} \tag{11}$$

$$\xi_S = \xi_{S0}-\frac{\xi_{S0}}{\xi_0}\left(\xi_0-\xi\right) \tag{12}$$

$$\xi_M = \xi_{M0}-\frac{\xi_{M0}}{\xi_0}\left(\xi_0-\xi\right) \tag{13}$$

σ_s^{cr} and σ_f^{cr} denote the initial and final stresses for the stress induced martensite (SIM) transformation during the $A \to M$ transformation. C_M and C_A are material properties associated to the relations between temperature and phase transformation stresses.

3. THE THERMOMECHANICAL MODEL OF THE SMA SPRING

A formulation for SMA springs was proposed by Liang and Rogers (1993). However, because of the limitations previously mentioned for this model, some modifications were considered in the present work in order to represent more realistically the mechanical behavior of these components. Such adjustments consist basically of employing the Liang and Rogers' SMA spring formulation adapted to conditions exhibited into Brinson's (1993) model. This means that some changes in terms of equations evolution, work temperatures and critical stress must be made.

According to Shigley *et al*. (2005) the maximum shear stress of a linear spring is given by:

$$\tau_{max} = K\frac{2FR}{\pi r^3} \tag{14}$$

where K is called the Wahl correction factor (considered equal to one by Liang-Rogers, 1993), F is the external force, R the mean springs radius and r the radius of the spring wire. The deflection of linear elastic spring can be found by considering the deformation of an element of length dx cut from a wire of radius r as showed in Fig. 1.
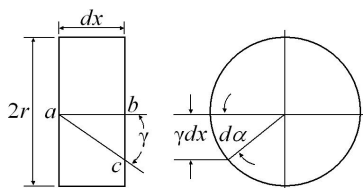
Figure 1. Cross-section of the helical spring element (Liang e Rogers, 1993).

The quantity γ denotes the angle originated from a spring torsion deformation and its equation is:

$$\gamma = \frac{\tau}{G} = \frac{2FR}{\pi r^3 G} \tag{15}$$

where G represents the shear modulus. The angle $d\alpha$ in which the section of the element rotates can be written as:

$$d\alpha = \frac{\gamma}{r} dx \tag{16}$$

and the angular deflection at a wire end in relation to other one is:

$$\alpha = \int_0^{2\pi RN} \frac{\gamma}{r} dx = \frac{4FR^2 N}{r^4 G} \tag{17}$$

where N is the number of active coils. Therefore, the total deflection is expressed as:

$$y = \alpha R = \frac{4FR^3 N}{r^4 G} \tag{18}$$

with the spring constant defined by:

$$k = \frac{r^4 G}{4R^3 N} \tag{19}$$

The elastic modulus of the SMA is function of ξ and according to Liang (1990) can be represented by:

$$D = D_A + \left(D_M - D_A\right)\xi \tag{20}$$

The relation between the elastic and shear modulii is:

$$G = \frac{D}{2\left(1+\mu\right)} \tag{21}$$

where μ is the Poisson's ratio. Considering the relation between normal and shear stresses as $D = \sqrt{3}\,G$ and supposing that the shear modulus only depends on total martensite fraction, the thermoelastic sensor and temperature are constant and all initial conditions are null, the Eq. (5) described by Brinson (1993) can be rewritten as:

$$\tau = G\gamma + \frac{\Omega}{\sqrt{3}}\xi_S + \frac{\Theta}{\sqrt{3}}(T - T_0) \tag{22}$$

The shear stress of a SMA coil can still be expressed from Equation (15) as:

$$\tau = \frac{2FR}{\pi r^3} \tag{23}$$

and the angle γ can be solved from Equation (22) resulting in:

$$\gamma = \frac{\tau}{G} - \frac{\Omega}{\sqrt{3}G}\xi_S - \frac{\Theta}{\sqrt{3}G}(T - T_0) \tag{24}$$

From Equations (17) and (18) it is possible to obtain the deflection of a SMA spring as:

$$y = \int_0^{2\pi RN} \frac{\gamma}{r} dx = \frac{2\pi R^2 N}{r}\left(\frac{\tau}{G} - \frac{\Omega}{\sqrt{3}G}\xi\right) \tag{25}$$

Substituting Equation (23) into Equation (25) yields:

$$y = \frac{4R^3 N}{Gr^4} F - \frac{2\pi R^2 N \Omega}{\sqrt{3} Gr} \xi \tag{26}$$

The Equation (26) above describes the load-deflection relation for SMA springs.

4. NUMERICAL SIMULATIONS

4.1. Symmetrical Rotating Model

The rotor system under analysis in this work (Figure 2) consists of a shaft of length 800 mm and 16 mm in diameter, two disks of 50 mm thick and outside diameter of 164 mm, positioned to l_1 and l_2 distances from ends. The constants of the shaft and disks dimensions are summarized in Fig. 2.

Parameter	Dimension (mm)
$l_1 = l_3$	250
l_2	300
d_d	164
d_s	16
t	50
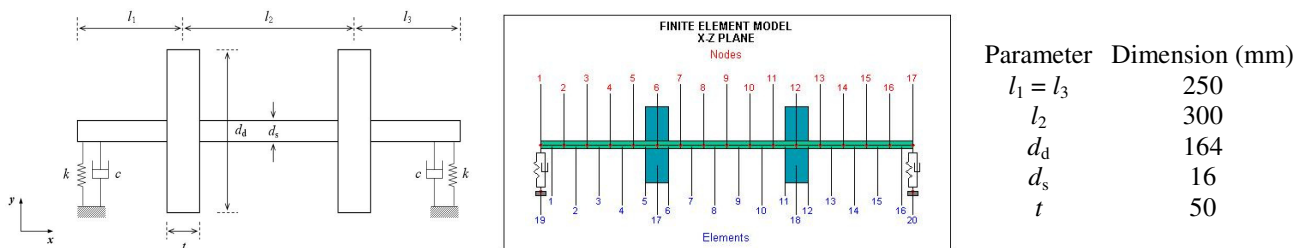
Figure 2. Schematic of rotor system with two disks and its main features.

Initially, the numerical complex response is computed employing a conventional bearing model, that is, bearings in which there is no SMA element inserted. A finite element model developed in MATLAB® code is used to determine the numerical response of the system, where the stiffness and damping constants for each bearing are $k_{yy} = k_{zz} = 10^5$ N.m^{-1} and $c_{yy} = c_{zz} = 2.5 \times 10^{-3}$ N.s.mm^{-1}. In this model, the cross stiffness and damping are null, i.e., $k_{yz} = k_{zy} = 0$ and $c_{yz} = c_{zy} = 0$. The shaft's and disks' properties are assumed to be: Young's modulus $E = 210$ GPa, specific mass $\rho = 7850 \times 10^{-9}$ kg.mm^{-3}, and Poisson's ratio $\mu = 0.3$.

The finite element model response is obtained in terms of natural frequencies (critical speeds) and mechanical unbalance, that is characterized by an eccentric mass $m = 3.05$ g placed in the radial position $\varepsilon = 82$ mm (node 6). The analyzed frequency range comprises the first two critical speeds of the system. Some changes have been made in order to build the numerical model with variable stiffness. First, a set of SMA springs was externally positioned at the right-hand end of the shaft and the modified bearing is schematically represented in Fig. 3.

Parameter	Not-activated Bearing Model	Activated Bearing Model
k_S	23 N.mm^{-1}	58.7 N.mm^{-1}
k_{EQ}	~23 N.mm^{-1}	~58.7 N.mm^{-1}
k	10^5 N.mm^{-1}	
c	2.5×10^{-3} N.s.mm^{-1}	
N	4	
R	6.85 mm	
r	1.85 mm	
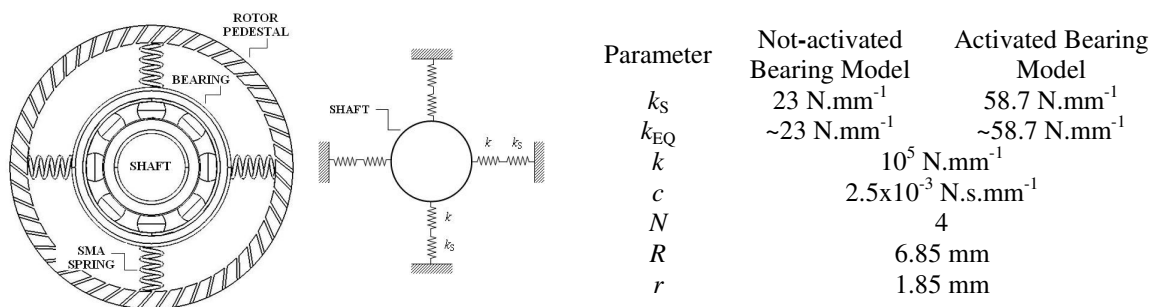
Figure 3. Representation of the bearing with SMA springs and conditions for the not-activation and activation states.

The values of SMA spring stiffness were obtained from Liang and Rogers' macro-mechanical model (Liang and Rogers, 1993). However, due to the limitations of this model, it was necessary to adapt this model to Brinson's conditions, i.e., some changes were made in terms of evolution equations, work temperatures and critical stresses. A numerical code written in MATLAB® environment was implemented for this purpose. These stiffness values are described in Fig. 3 for the two thermomechanical states. The equivalent stiffness (k_{EQ}) resulting of the association of springs in series (where k and k_S are respectively the bearing's and spring's stiffnesses) is also showed in this figure. The principle considered for spring activation and de-activation is based on the Active Property Tuning method (APT), in which only changes in the SMA material properties are took into account (Zak et al., 2003).

For this simulation, two points of the finite element model are analyzed. The first one is the node 17 (spring) that is used to verify whether the SMA spring deflection is within the elastic range (see the section 5.1). The second point is

the node 6 (disk) that is used to analyze the influence of SMA spring activation and de-activation processes on the vibration amplitude of the system.

4.2. Asymmetrical Rotating Model

The second finite element model has been developed with the same physical configuration than the first one. Nevertheless, the disks have been positioned at non-symmetric location in relation to the ends. For this model $l_1 = 400$ mm and $l_3 = 150$ mm. We also considered different stiffnesses in the y and z directions of the SMA bearing ($k_{EQyy} = 23$ N.mm^{-1} and $k_{EQzz} = 28$ N.mm^{-1}). Hence, this arrangement is able to stimulate the arising of the backward whirling, which is a quite dangerous precessional motion and causes cyclical stresses in the rotor system. Such a configuration also enables the arising of mixed operational modes that can be as hazardous as the backward whirling.

An appropriate way to visualize how each station of the rotor whirls when it is subjected to unbalance forces is through the SDI (Shape and Directivity Index) Plot or 3D SDI (Dias Jr. and Allemang, 2000). This plot is built by computing the SDI for all nodes and each rotational speed. Specific colors are assigned to each SDI value and a convenient color map must be used in order to be possible to easily distinguish between backward and forward precessional motion of the stations of the rotor. The SDI is mathematically defined by (Han and Lee, 1998) as:

$$-1 \leq SDI = \frac{|P_f| - |P_b|}{|P_f| + |P_b|} \leq 1 \tag{27}$$

where P_f and P_b are the vectors that describe the forward and backward precessional motions respectively. The relationships between the values of the SDI, the shape of the orbit of a station of the rotor and the direction of the precessional motion are defined by Han and Lee (1998) as following:

- SDI = -1 → Circular backward precessional motion;
- -1 < SDI < 0 → Elliptical backward precessional motion;
- SDI = 0 → Rectilinear motion;
- 0 < SDI < 1 → Elliptical forward precessional motion;
- SDI = 1 → Circular forward precessional motion.

The sign of the SDI defines the direction of the precessional motion while the shape of the orbit is defined by its absolute value (Dias Jr. and Allemang, 2000). Finally, the numerical model is again submitted to activation process and in this situation the system becomes an isotropic one. The values of the equivalent stiffness coefficients in the y and z directions of the SMA bearing are: $k_{EQyy} = k_{EQzz} = 58.7$ N.mm^{-1}. The numerical response of the model has been plotted in terms of its critical speeds, operational modes and vibration amplitudes due to mechanical unbalance induced by a unbalance mass $me = 250$ g.mm is applied at both disks.

5. RESULTS

5.1. Thermomechanical Behavior of the SMA Spring

In this section we present the numerical simulations of the SMA spring behavior for the two thermomechanical states (martensite and austenite). By means of the isothermal curves it is possible to identify the elastic ranges in which the SMA spring behavior is valid in this work. The material parameters for this numerical simulation are defined by Liang (1990) and Brinson (1993) as being: $M_f = 282$ K, $M_S = 291.4$ K, $A_S = 307.5$ K, $A_f = 322$ K, $D_M = 26.3$ GPa, $D_A = 67$ GPa, $C_M = 8$ MPa, $C_A = 13.8$ MPa, $\varepsilon_L = 0.067$, $\Theta = 0.55$, $\sigma_s^{cr} = 100$ MPa and $\sigma_f^{cr} = 170$ MPa.

Figure 4 shows the load-deflection and stress-strain plots with the elastic ranges for the martensite and austenite phases below M_f ($T = 278$ K) and above A_f ($T = 333$ K) respectively. When the SMA spring is in the martensite state the maximum elastic deflection supported by it is $y_M = 3.64$ mm and the corresponding load is 83.83 N. On the other hand, in the austenite state, the maximum deflection is $y_A = 6.19$ mm and the load is 363 N. The stiffnesses for these states are 23 N.mm^{-1} and 58.7 N.mm^{-1}, respectively. There is a residual deflection in the low-temperature curve due to the quasiplastic behavior of the SMA spring. The high-temperature curve in turn shows the superelastic behavior of the SMA springs, where the stress induced martensite (SIM) is accomplished and there is no residual deformation.

As far as the martensite fraction variation with the load is concerned, Fig. 5 shows five isothermal curves that include different points on the SMA spring transformation: $T < M_f$ ($T = 278$ K), $M_f < T < M_S$ ($T = 287$ K), $M_S < T < A_S$ ($T = 301$ K), $A_S < T < A_f$ ($T = 315$ K), $T > A_f$ ($T = 333$ K). In the case of the single-variant martensite all the curves present a null initial martensite because of the load is also null. On the other hand, the multi-variant martensite fraction depends on the work temperature and decreases as the load is applied.
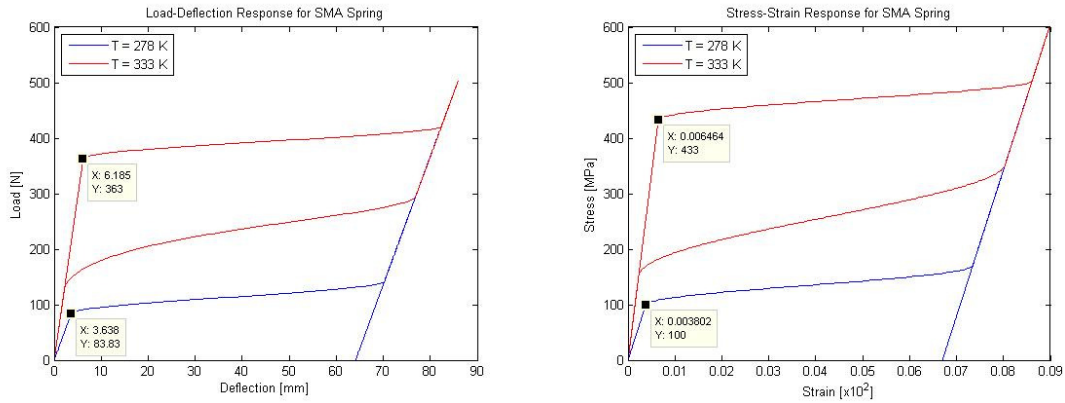
Figure 4. Isothermal load-deflection and stress-strain curves for SMA spring. The highlighted points represent the elastic limits in which the SMA behavior is valid for this work.
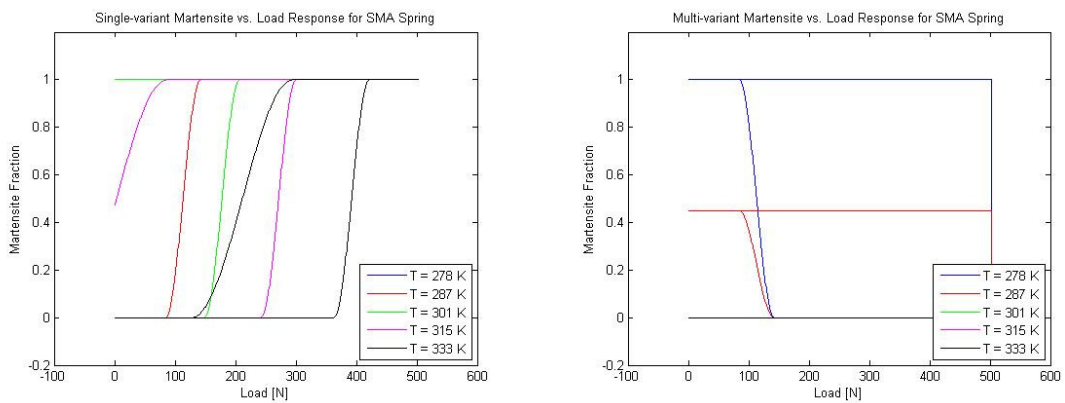
Figure 5. Isothermal martensite fraction *vs*. load curves for SMA spring.

5.2. Symmetrical Rotating Model

In the first case study it is shown how an adaptive vibration control with SMA springs can be used for reducing vibration levels of rotating systems. The symmetrical model described in section 4 is used and the comparisons are made with the vibration amplitudes measured at nodes 6 and 17. In this case it is assumed that the system has two operating frequencies: 11.67 Hz and 23.58 Hz. In the case of the conventional bearing model, the displacement amplitudes in these frequencies are 4.36 mm and 0.012 mm for node 6 and 1.02×10^{-3} mm and 1.23×10^{-5} mm for node 17, respectively (Fig. 6). The first amplitude (node 6) is very high because it coincides with the first critical speed of the system.
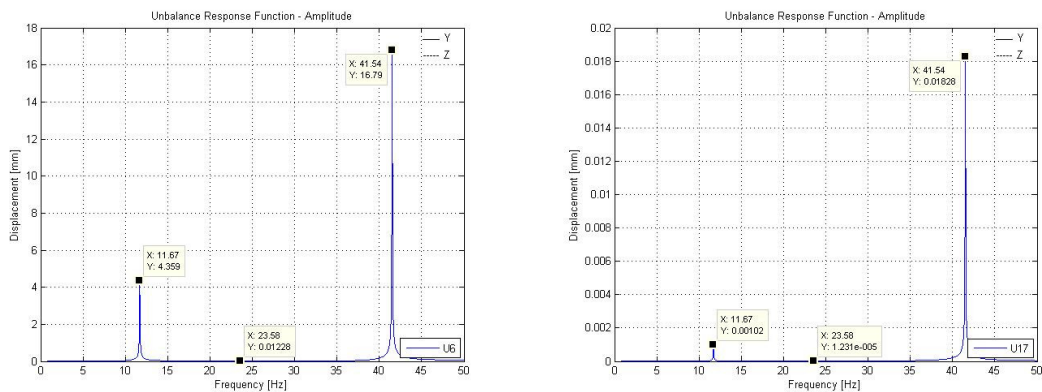
Figure 6. Unbalance response measured at nodes 6 (disk) and 17 (spring) respectively for the symmetric model with conventional bearing.

In relation to the amplitudes calculated at node 17 for the models with the not-activated and activated springs, the vibration amplitudes for the two operating frequencies are within the elastic ranges (y_M = 3.64 mm and y_A = 6.19 mm) (Figs. 7 and 8). It is important to emphasize that the aim in this work is to explore only the stiffness change through temperature change, not the shape memory or pseudoelastic effects.

At node 6 the amplitudes with the not-activated springs in the operating frequencies are 0.013 mm and 0.021 mm (Fig. 7). In this situation, there was a reduction of 99.7 % in the magnitude of vibration at the first operational frequency, but in the second operational frequency the level of vibration increased in 75 %. In the case of the model with the activated springs the amplitudes of the first disk in the operating frequencies become 0.035 mm and 0.0037 mm, respectively. Compared to model with conventional bearing, the level of vibration due to activation of SMA springs decreased for the two operating frequencies (99.2 % and 69.2 %, respectively). On the other hand, when compared to the model with not-activated bearing, there was an increase (169.2 %) in the magnitude of vibration at the first operational frequency but in the second one the level was reduced in 82.4 % (Fig. 8). Thus, for the last situation, the correct manner of operation is to use the SMA springs disabled when operating in the first frequency of work and use the springs activated when operating in the second frequency of work.
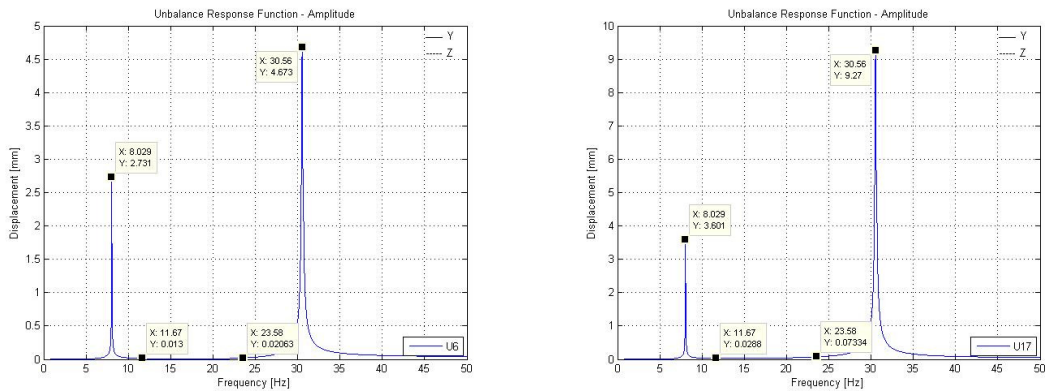
Figure 7. Unbalance response measured at nodes 6 (disk) and 17 (spring) respectively for the symmetric model with not-activated bearing.
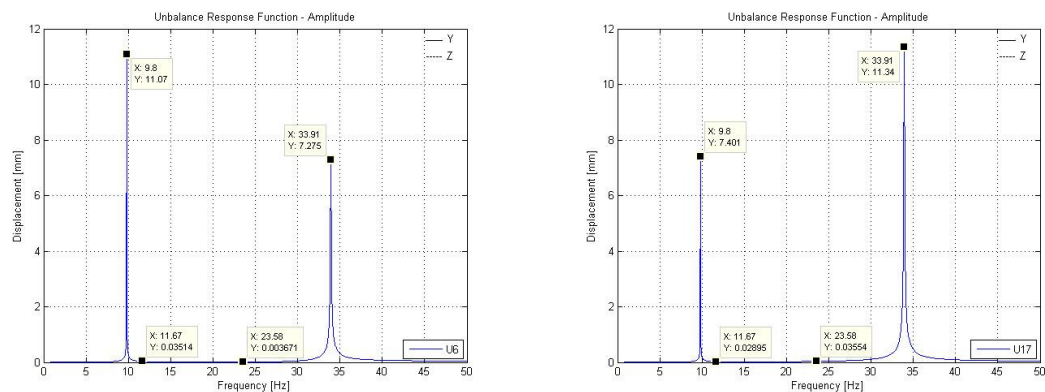
Figure 8. Unbalance response measured at nodes 6 (disk) and 17 (spring) respectively for the symmetric model with activated bearing.

5.3. Asymmetrical Rotating Model

Regarding the asymmetrical model and the new configuration imposes on it, we are able to detect the presence of backward whirling by means of unbalance response function (measured at node 14) shown in Fig. 9. The backward whirling appears in dashed line and forward whirling in solid line. In this case, as the system is anisotropic, there are also the critical speeds that correspond to coincidence between the operational speed and the backward natural frequencies.

The 3D SDI shown in Fig. 9 shows that for the analyzed frequency range the model is in backward whirling (in ~7.5 Hz) and in mixed whirling (in ~26-27 Hz), that is, some rotor stations are in forward whirling and others ones are in backward whirling simultaneously. The forward whirling is dominant in the considered frequency range.
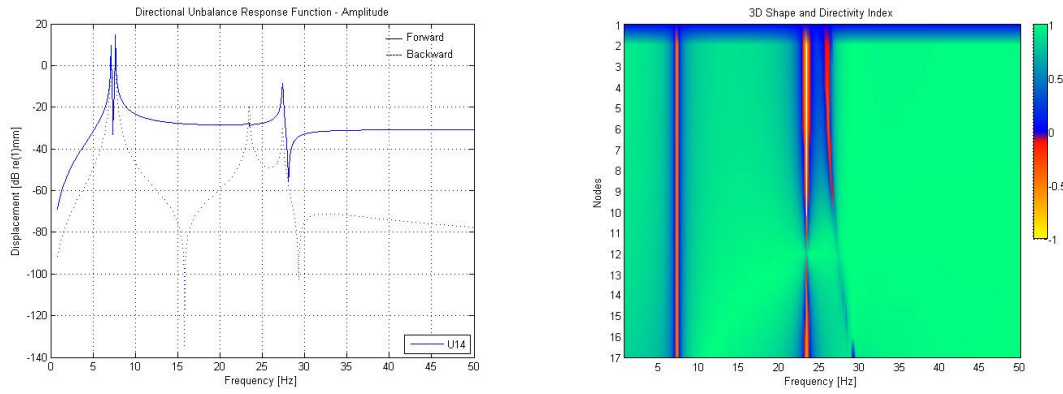
Figure 9. Unbalance response for the asymmetric model with not-activated bearing and 3D SDI for the asymmetric model with not-activated bearing.
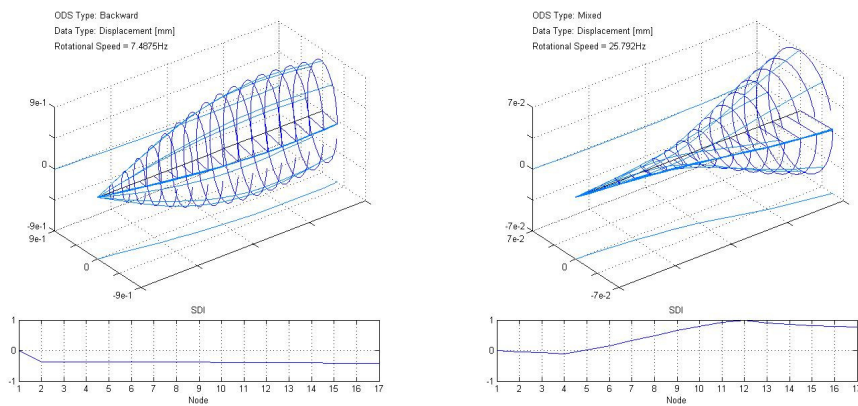
Figure 10. Operational deflection shape type elliptical-backward in 7.49 Hz and operational deflection shape type mixed in 25.79 Hz.
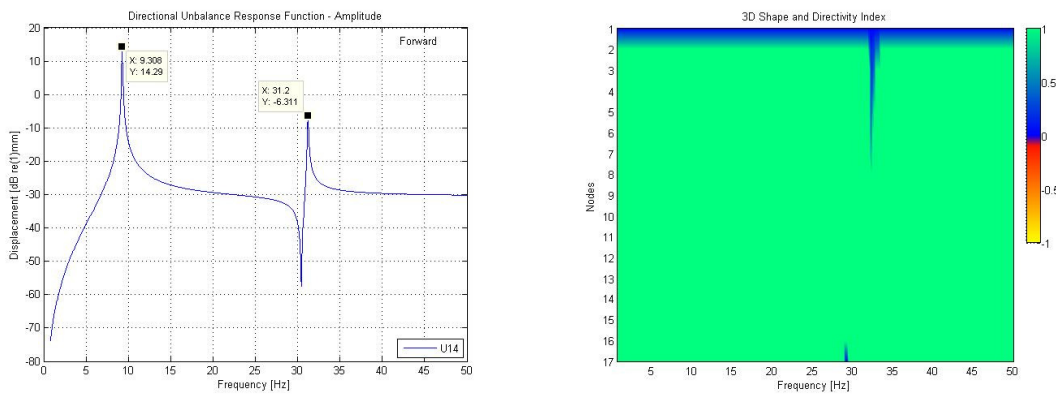
Figure 11. Unbalance response for the asymmetric model with activated bearing and 3D SDI for the asymmetric model with activated bearing.

In Figure 10 we can observe the operational deflection shape (ODS) of the backward precessional motion at 7.49 Hz. All the rotor stations are under elliptical whirling, i.e., the $-1 < SDI < 0$. In this figure we can also notice the operational deflection shape of the mixed precessional motion at 25.79 Hz. We can also notice the stations moving in forward whirling (nodes 5 to 17) present higher amplitudes in comparison to ones moving in backward whirling (nodes 1 to 4). Besides, one rotor station describes a circular motion (node 12) while others ones describe an elliptical motion.

Upon SMA springs activation process, the forced response has been measured at node 14 and is described in Fig. 11. As mentioned in previous sections, the model becomes an isotropic system. In this plot, the whole backward frequency range has been suppressed, and the only precessional motion encountered is the forward one. It means that the SMA springs may be an exploited successfully for controlling two hazardous rotational motions, as previously mentioned.

Finally, the 3D SDI for the asymmetric model with activated bearing (Fig. 11) confirms that there is only forward whirling in the range between 0 and 50 Hz. Moreover, almost all the rotor stations are in the condition SDI = 1, that is, whirling happens in a circular manner.

6. CONCLUDING REMARKS

This paper has addressed some basic aspects of the application of SMA in adaptive vibration control of rotating machinery. The methodology of control is to use springs made of shape memory alloy (SMA) connecting them to one of the bearings of the system and using the control process properly. When the springs are activated, which correspond to be heated, there is a solid phase transformation. This phase transformation corresponds to change of the martensite into austenite phase. In this case the elasticity modulus is increased and consequently the stiffness is also increased.

In the first part of this work some numerical simulations have been performed in order to predict the SMA spring behavior and obtain the stiffness of this component in the elastic range for martensite and austenite phases. A well-know macro-mechanical constitutive models have been together employed for this purpose.

As case studies, two rotating systems are presented: the first one is a symmetrical (isotropic) model and the second is an asymmetric (anisotropic) model. In the first case, it is shown how the activation of the springs can reduce the amplitude levels of vibration subject to unbalance forces. In the last case, due the anisotropy and others parameter of the system, the results presented a range of frequency of backward precession and also operational mixed modes appear. Then, with the activation of the SMA springs the whirling movement of the rotor becomes fully of forward type.

7. ACKNOWLEDGMENTS

8. REFERENCES

Auricchio, F., Taylor, R.L., Lubliner, J., 1997, "Shape-Memory Alloys: Macromodelling and Numerical Simulations of the Superelastic Behavior", Computional Methods Applied to Mechanical Engineering, Vol. 146, pp. 281-312

Brinson, L.C., 1993, "One-dimensional Constitutive Behavior of Shape Memory Alloys: Thermomechanical Derivation with Nonconstant Material Functions and Redefined Martensite Internal Variable", Journal of Intelligent Material Systems and Structures, Vol. 4, pp. 229-242.

Dias Jr., M, Allemang, R.J., 2000, "Some Insights into the Simultaneous Forward and Backward Whirling of Rotors", Proceedings of the 20th IMAC.

Han, Y., Lee, C., 1998, "Directional Wigner Distribution for Order Analysis in Rotating/Reciprocating Machines", Mechanical Systems and Signal Processing, Vol. 13, No. 5, pp. 723-737.

He, Y.Y., Satoko, O., Chu, F.L, Li, H.X., 2007, "Vibration Control of a Rotor-bearing System Using Shape Memory Alloy: I – Theory", Smart Materials and Structures, Vol. 16, pp. 114-121.

He, Y.Y., Satoko, O., Chu, F.L, Li, H.X., 2007, "Vibration Control of a Rotor-bearing System Using Shape Memory Alloy: II – Experimental Study", Smart Materials and Structures, Vol. 16, pp. 122-127.

Iwata, Y., Nonami, N., 1983, "Vibration Control of Rotating Shaft with Self-optimizing Support System, Transactions of Japanese Society of Mechanical Engineering (JSME) C, Vol. 49, pp. 1897-1903.

Liang, C., 1990, "Constitutive Modeling of Shape Memory Alloys", Ph.D. dissertation, Departament of Mechanical Engineering, Virginia Polytechnic Institute and State University, Blacksburg, VA.

Liang, C., Rogers, C.A., 1990, "One-Dimensional Thermomechanical Constitutive Relations for Shape Memory Materials", Journal of Intelligent Material Systems and Structures, Vol. 1, No. 2, pp. 207-234.

Liang, C., Rogers, C.A., 1993, "Design of Shape Memory Alloy Springs with Applications in Vibration Control", Journal of Vibration and Acoustics, Vol. 115, pp. 129-135.

Shigley, J.E., Mischke, C.R., Budynas, R.G., 2005, "Mechanical Engineering Design", 7th ed., McGraw-Hill, Inc.

Tanaka, K., 1986, "A Thermomechanical Sketch of Shape Memory Effect: One-dimensional Tensile Behavior", Res. Mechanica, International Journal of Structural Mechanics and Materials Science, Vol. 18, No. 3, pp. 251-263.

Zak, A.J., Cartmell, M.P., Ostachowicz, W.M., 2003, "Dynamics and Control of a Rotor Using an Integrated SMA/Composite Active Bearing Actuator", Key Engineering Materials, Vols. 245-246, pp. 233-240.

9. RESPONSIBILITY NOTICE

The authors are the only responsible for the printed material included in this paper.